Photodynamics of Latex Nanospheres Examined Using Two-Photon Fluorescence Correlation Spectroscopy

R. Goyan, R. Paul, and D. T. Cramb*

Department of Chemistry, University of Calgary, 2500 University Drive NW, Calgary, AB, T2N 1N4, Canada

Received: July 24, 2000; In Final Form: October 18, 2000

Fluorescence correlation spectroscopy (FCS) is a highly sensitive and selective technique with which one can analyze highly localized environments using the fluctuations in the average fluorescence of a probe fluorophore. Two-photon FCS has been proposed as a method to minimize photodamage to the probes and living organisms under observation. While multiphoton excitation reduces photodamage outside the focal volume, photodynamic effects within the volume can be substantial. The dynamics occurring in the focal excitation volume of a two-photon confocal microscope are examined using FCS of dye-loaded, 100 nm diameter polystyrene spheres. Multiphoton photodynamic events are observed which cannot be explained either by simple local solution heating or by intersystem crossing within a single excited dye molecule. The laser power dependence of photodynamics process suggests that a four-photon absorption by polystyrene and subsequent ablation of the sphere is the mechanism of fluorescence-reducing photodamage.

Introduction

Fluorescence correlation spectroscopy (FCS) was first introduced in the early 1970s.[1] The technique analyzes the fluctuations in the average fluorescence of a system under observation. It is a very attractive technique, as it has high sensitivity and selectivity, is rapid, and requires a minimal sample volume.[2] While FCS was originally used to quickly determine the concentration, diffusion coefficients, and chemical rate constants of molecules in solution,[1] FCS has found application in a wide variety of areas. FCS is commonly used at the single-molecule level of detection.[3] Essentially, any process that will change the intensity of fluorescence in the system can be monitored using FCS. FCS has been used to measure triplet-state parameters,[4] give information on intracellular environments and reactions at cell surfaces,[5−7] monitor hybridization,[8] detect HIV-1 RNA,[9] monitor ion concentration,[10] study PNA−DNA interactions[11] and DNA binding,[12] probe intranuclear diffusion,[13] measure polydispersity,[14] establish binding strength,[15] evaluate photodynamic properties,[16] and observe conformational dynamics.[17]

The vast majority of these experiments have been performed using one-photon excitation with either a HeNe or an Ar^+ ion laser. However, these measurements may contribute to substantial photobleaching or photodestruction of the fluorescent probe. In addition, survival of living organisms may be influenced by the use of one-photon excitation. Two-photon excitation has been proposed as a method to minimize the damage to living organisms during FCS measurements by confining excitation to a small focal volume.[5,18,19] Two-photon excitation also has advantages due to the elimination of out-of-focus background, the avoidance of Raman and Rayleigh scattering to reduce in-focus background, and the elimination of a pinhole from the detection system, reducing alignment challenges. However, because different excited states may be reached with two-photon excitation, in-focus photobleaching may be reduced, eliminated, or even enhanced.

Although multiphoton excitation reduces photodamage outside the focal volume, photodynamic effects within the volume can be significant. For single molecules, irreversible two-photon initiated photodamage has been observed.[20] Even at a modest mean power for pulsed femtosecond lasers (10 mW), terawatts of peak power (10^{12} W/cm^2) can be generated via the severe focusing used in multiphoton imaging. Indeed, at power levels $\geq$10 mW Chinese hamster ovary cells have been observed to fragment.[21] Moreover, living cells optically trapped with cw near-infrared light (760−800 nm) were found to develop compromised reproductive capabilities owing to multiphoton absorption events.[22]

Near-infrared lasers have also been used for trapping 1−4 μm microspheres.[23] In ref 23, Zhang et al. observed multiphoton fluorescence excitation even in cw infrared trapped fluorescently labeled spheres. Previous work by Misawa et al.[24] examined the effect of high-power pulsed infrared lasers on trapped microspheres ($\sim$6 μm diameter). They observed that a minute hole could be fabricated in the trapped sphere using a single laser shot. Multiphoton absorption by polystyrene was suggested to be the mechanism for the ablation of material from the latex sphere.

From the above examples, it is clear that while two-photon excitation does minimize some of the problems associated with one-photon excitation, there may be other considerations with nonlinear excitation. Therefore, the dynamics occurring in the focal excitation volume of multiphoton microscopes must be examined in greater detail. We have employed two-photon FCS on solutions of polystyrene nanospheres small enough ($\sim$100 nm diameter) that optical trapping should be minimized. These spheres are advantageous as model systems because their diffusion coefficients are calculable and the dye is protected from environmental effects. We have examined the laser power dependence on the sphere dynamics within the excitation volume and have observed multiphoton photodynamic effects that cannot be explained simply by local solution heating. Moreover, we have extended the two-photon FCS theory developed by Berland et al.[5] to include terms that represent these dynamic effects.

10.1021/jp0026235 CCC: $20.00
Published on Web 03/03/2001

Experimental Section

FCS Instrumentation. FCS measurements were performed using a home-built instrument. The 532 nm output of a Millennia V diode-pumped Nd:YVO_4 cw laser (Spectra-Physics, Mountain View, CA) set at 5 W was used to pump a model 3941-M1S Tsunami fs mode-locked, tunable Ti:sapphire laser (model 3941-M1S, Spectra-Physics), operating at 82 MHz. The laser light was analyzed using a Laser Spectrum Analyzer (model E200, IST-REES). The beam was steered onto a 3 mm aperture using ultrafast mirrors (Melles Griot, Irvine, CA) to minimize pulse broadening. From the spectral width of the laser light, we estimate the temporal pulse width to be 40 fs before entering the microscope. A polarizing prism was used to control the intensity of the beam. The beam cross-section was adjusted using a Galilean beam expansion system to ensure that it filled the back aperture of the microscope objective (100×, Plan-apochromat. N.A. 1.4, oil immersion, Carl Zeiss Canada, Don Mills, ON). The beam entered the Zeiss Axioplan 2 microscope and was then reflected by a dichroic mirror (560DCSP Special, Chroma Technology Corp., Brattleboro, VT) through to the compound objective lens. The objective collected the fluorescence and passed it through the dichroic filter and then through a band-pass filter (F70−550, CVI Laser Corporation, Albuquerque, NM). The collected fluorescence light was detected by a photomultiplier tube (type R5600P, Hamamatsu Photonics K.K., Japan). The electrical signal was sent to a home-built current/voltage converter/amplifier which converted the signal to a usable format for the SR-400 two-channel gated photon counter (Standford Research Systems, Sunnyvale, CA). The photon counter was outfitted with a home-built circuit to obtain a TTL output signal. The TTL signal was sent to a hardware autocorrelator card (ALV-5000/E, ALV-GmbH, Langen, Germany, version 1.4.8.3) controlled by a Pentium computer. This card calculated the normalized fluorescence autocorrelation function.

The power of the beam before entering the objective was varied between 32 mW and 125 mW. This allowed the observation of signal under conditions of both high and low photobleaching. The actual power in the focal volume would be lower due to losses from the objective. The light intensity at the beam focus was not measured but is estimated to be 50% of that at the back aperture, owing to reflection losses off of the compound lenses.

Sample Preparation. The samples used were FluoSpheres carboxylate-modified, 0.1 μm diameter, rhodamine dye-filled orange microspheres (F-8800, Molecular Probes, Eugene, OR) with a fluorescence maximum at 560 nm. The spheres were diluted in 0.055 M phosphate buffer, pH 6.8, to a concentration of 4.3×10^{12} particles/mL. Polydispersion results using dynamic light scattering confirmed the average sphere diameter of a diluted orange sphere solution to be around 0.1 μm, thus no filtering seemed necessary. Dynamic light scattering was also used to confirm the expected diffusion coefficient of the spheres. The solutions were sonicated for 1 h and allowed to cool before being sealed in a three-well microscope slide. Fluorescence emission and fluorescence excitation spectra were measured using a spectrofluorimeter (Photon Technology International (Canada) Inc., London, ON). FCS of the spheres was run at a two-photon excitation wavelength of 780 nm.

FCS Experiments. Because the FluoSpheres have a well-defined radius, we used the spheres themselves to optimize and calibrate our instrumentation. A small amount of sonicated, cooled sample solution was placed in the center well of a three-well microscope slide. A cover slip of 0.13−0.16 mm thickness (Corning Brand, No.1, VWR Canlab, Mississauga, ON) was sealed on the slide with mounting medium (Cytoseal 280, VWR) which gave the best seal, thus preventing the formation of air bubbles. Each experiment was performed several times to ensure consistency. The background noise level was adjusted to be less than 100 Hz (using the SR400 discriminator), while the signal levels were between 10 kHz and 1 MHz. FCS collection times ranged from 10 s to several minutes, depending on the signal level. A good run was defined as one for which the count function looked random, with no evidence of aggregation-induced intensity spikes. An example of a count rate versus time histogram is given in Figure 1.

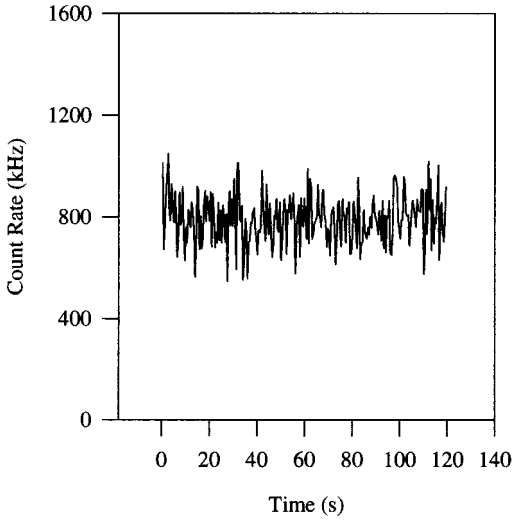

Figure 1. Example of a count rate versus time. This count rate histogram was recorded for a laser power of 115 mW. The background counts were less than 100 Hz.

Theoretical Considerations

Laser Intensity. The spatial profile of a focused laser beam is described by an intensity distribution function which is radially (r) Gaussian and axially (z, propagation direction) Lorentzian. Thus, the overall intensity distribution is given by[25]

$$I(r,z) = \frac{2I_0\omega_0^2}{\pi\omega^2(z)} \exp\left(-\frac{2r^2}{\omega^2(z)}\right) \quad (1)$$

where

$$\omega^2(z) = \omega_0^2\left(1 + \left(\frac{z}{z_r}\right)^2\right) \quad \text{and where} \quad z_r = \frac{\pi\omega_0^2}{\lambda} \quad (2)$$

I_0 is the laser intensity, ω_0 is the beam waist, λ is the laser wavelength and z_r is also known as the depth of focus.

Fluorescence Autocorrelation Functions (ACFs). The normalized autocorrelation functions were analyzed using a modification of the formalism introduced by Berland et al.[5] In the absence of photodynamic effects, the two-photon autocorrelation function represents only diffusional phenomena. In this case, the form of the normalized function is obtained via normalizing the autocorrelation function presented by Berland et al.[5] Thus, to obtain the normalized ACF,

$$G(\tau) = \frac{2\alpha^2 I_0^4\,\omega_0^6}{\lambda^2\sqrt{4\pi D\tau}}\langle c\rangle g(D,\tau) \quad (3)$$

is divided by $\langle F\rangle^2$, where

$$\langle F\rangle = \frac{\alpha I_0^2 \omega_0^4 \pi}{\lambda}\langle c\rangle \tag{4}$$

c is the concentration of the fluorophore, τ is the lag time, α represents collection geometry and efficiency and D is the fluorophore's diffusion coefficient. Thus, the normalized autocorrelation function for pure diffusion is

$$G_D^N(\tau) = \frac{128}{\omega_0^2 \pi^3 \langle c\rangle \sqrt{(4\pi)^3 D\tau}} g(D,\tau) \tag{5}$$

where $g(D,t)$ is the integral

$$g(D,t) = \int_{-\infty}^{\infty} \mathrm{d}p \frac{\exp(-z_r^2 p^2/2D\tau)}{p^4 + (2 + 16D\tau/\omega_0^2)} \times \left[\frac{2p^2 + \frac{16D\tau}{\omega_0^2} - 4}{\sqrt{2}(2+p^2)} + \frac{2}{\left(2 + p^2 + \frac{16D\tau}{\omega_0^2}\right)^{1/2}}\right] \tag{6}$$

and p is the variable of integration. Equation 6 must be computed numerically.

From eq 5, one observes that the autocorrelation function at time zero gives a direct estimate of the number of molecules in the sample volume. Since the concentration is fixed in our experiments, changes in $G_D^N(0)$ can be related to the changes in the excitation volume as a function of increasing laser power.

If one suspects that a destructive, nonreversible chemical reaction is occurring within the transit time for diffusion through the excitation volume, then a term in the equation of motion for fluorophore concentration must be added. The equation of motion becomes

$$\frac{\partial}{\partial t'}\delta c(\vec{r}',t') = D\nabla^2 \delta c(\vec{r}',t') - k_{\mathrm{PD}}\delta c(\vec{r}',t') \tag{7}$$

Where $\vec{r}'$ is the three-dimensional position coordinate of the diffusing particle, c is the concentration, and k_{PD} is the rate constant for the process. The autocorrelation function thus becomes

$$G_{\mathrm{total}}^N(\tau) = G_D^N(\tau)\cdot \mathrm{e}^{-k_{PD}\tau} \tag{8}$$

It is interesting to note that this result parallels that of Palmer and Thompson[26] for one-photon FCS where they considered diffusion and a simple, fluorescence-reducing equilibrium. Palmer and Thompson found that the diffusion ACF could simply be multiplied by a term including the chemical dynamics. Moreover, if one argues that the equilibrium constant for the Palmer and Thompson's reaction is large, then their ACF simplifies to the diffusion contribution, multiplied by an exponential decay.

It is possible that the diffusing particles also experience flow directed along the direction of laser propagation. This could arise from radiation pressure,[27] where the net vector of radiation momentum is in the direction of laser propagation. In this case, eq 7 is modified to contain a term representing the velocity, v, along the z' direction.

$$\frac{\partial}{\partial t'}\delta c(\vec{r}',t') = D\nabla^2 \delta c(\vec{r}',t') - v\frac{\partial}{\partial z'}\delta c(\vec{r}',t') \tag{9}$$

Using this to solve for the autocorrelation function we obtain

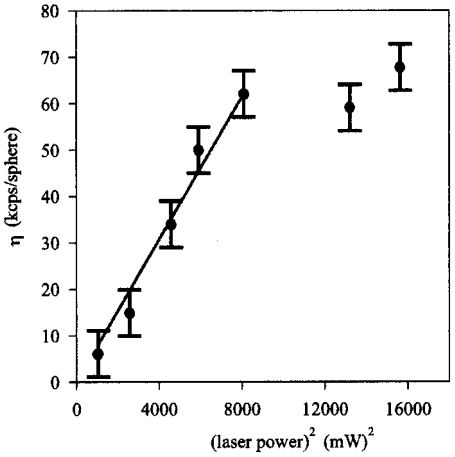

Figure 2. Normalized fluorescence intensity (kilocounts/sphere) as a function of laser power squared. See text for the normalization procedure.

$$G_{\mathrm{total}}^N(\tau) = G_D^N(\tau)\mathrm{e}^{-v^2\tau/4D} \tag{10}$$

It is important to note that eq 10 holds for $|z'/\tau| \gg |v|$, which will be true for velocities of the order $10^{-5}-10^{-6}$ m/s and values of $z' \neq 0$. This is the case for diffusion near the axial boundaries of the excitation volume, where diffusion along the z' direction dominates the long lag time decay of the ACF. Near $z' = 0$, lateral diffusion dominates the decay of the ACF. The derivations for eqs 8 and 10 and are presented in the Appendix.

In all instances, the correlation functions were fitted employing a Levenberg−Marquardt algorithm using eqs 5, 8, or 10, where appropriate. In all cases, the $g(D,t)$ integral was fit numerically for each iteration because changes in ω_0 affect its value. The value of the diffusion coefficient, D, was held fixed for all fits. Thus, when eq 5 was used, ω_0 was floated and when eqs 8 or 10 were used, ω_0 and k_{PD} or v were floated, respectively.

Functionally, eqs 8 and 10 are the same. It is therefore impossible to conclude whether unidirectional chemical kinetics or flow is occurring solely based on the shape of the measured ACF. One must examine the consistency of the rate constants and velocities and their laser power dependencies to assess the exclusivity of these two phenomena.

Results and Discussion

Saturation of Two-Photon Excitation. We present the normalized fluorescence intensity as a function of laser power squared in Figure 2. Similar to Schwille et al.,[19] we normalize the fluorescence intensity to η, the intensity per fluorescing particle (in this case, per sphere). This is accomplished through multiplying the intensity by the zero time intercept of the autocorrelation function $G_D^N(0)$, which is analogous to dividing by the number of particles in the excitation volume. From Figure 2, we note that we are in the linear regime for 32−90 mW and appear to approach the saturation threshold thereafter. The linear regime is consistent with ref 5, where small nanospheres were also employed. The saturation we observe occurs at higher laser power than that observed for tetramethyl rhodamine by Schwille et al.[19] This is presumably because of the difference in dye molecule. Finally, because the emission spectrum of the orange spheres does not overlap with the laser wavelength (780 nm), we do not anticipate any significant simulated emission.

Excitation Threshold Waist. The nonlinear least-squares fit of eqs 5, 8, or 10 to the autocorrelation function allows the

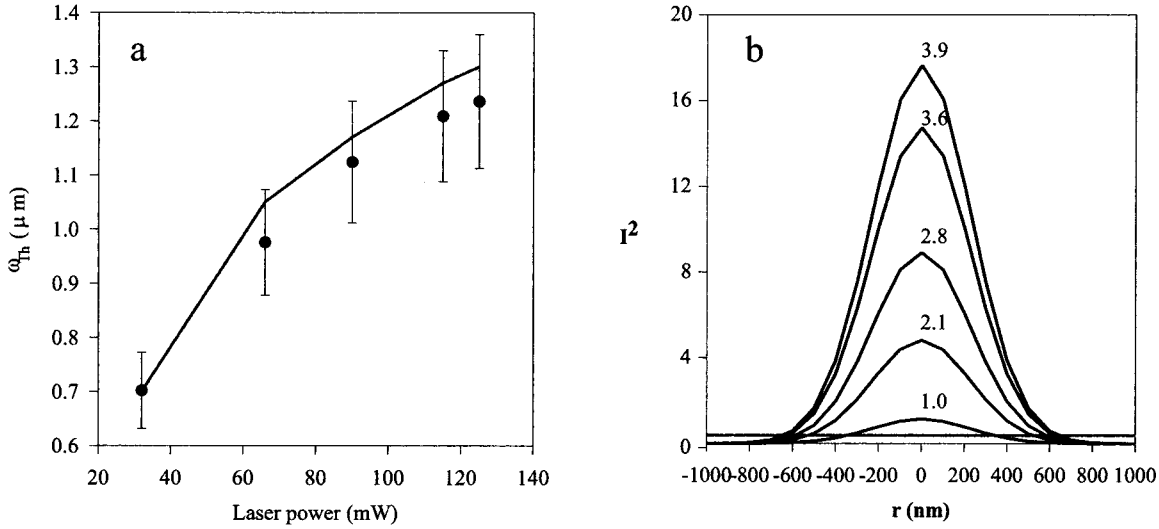

Figure 3. (a) Values of the excitation threshold waist, ω_{Th},versus laser power. (b) Normalized squared Gaussian intensity functions versus radial position, r, at an axial position of $z = 0$. The numbers near the peaks of the functions are the relative powers of the incident laser. The horizontal line near the bottom represents the threshold squared power value for two-photon excitation.

TABLE 1

power	ω_{Th} (mm)	k_{PD} (s^{-1})	v (m/s)
32	0.70	0.0	0.0
66	0.97	1.00	0.44
90	1.12	4.34	0.92
115	1.21	7.69	1.22
125	1.24	14.29	1.67

recovery of a beam waist, ω_0. ω_0 is twice the distance from the beam center to where the Gaussian radial intensity distribution falls to $1/e^2$ of its maximum value and thus should not be a function of laser intensity. However, the absolute intensity at ω_0 does change as a function of laser intensity. Furthermore, one can consider the existence of a finite threshold laser intensity for two-photon excitation.[18] It is this excitation threshold that confines two-photon excitation to a finite volume with a finite waist. As the applied laser intensity increases, the threshold waist, ω_{Th}, will become larger. The effect of this would be an *apparent* change in ω_0. We have therefore chosen to model the change in threshold waist, by allowing ω_0 to float in our fitting procedure. There are two parts of the ACF, which help determine ω_0. These are the zero lag time intercept and the transit time through the excitation volume, given a constant diffusion coefficient. As laser power is increased, the excitation volume increases for two-photon absorption. This is clear from our $G_D^N(0)$ values, which become smaller as laser intensity is increased, suggesting that there are more spheres in the excitation volume.

The values of ω_{Th} versus laser power can be found in Table 1 and plotted in Figure 3a. In Figure 3a, we have also included a plot of the predicted value of ω_{Th} based on the square of eq 1. To do this prediction, we chose the lowest power value (i.e., $I_0 = 32$ mW) and plotted the square of eq 1 as a function of radius, r. This plot can be found in Figure 3b. One can then set the threshold value for excitation such that the threshold beam waist of 700 nm (i.e. ω_0 for 32 mW) is recovered. Next, the square of eq 1 is replotted at the increasing values of laser power (i.e., with $I_0 = 66$, 90, 115, 125 mW). Since the threshold intensity is constant, the threshold beam waist values increase. This is shown diagrammatically in Figure 3b where the horizontal threshold line crosses the intensity-squared plots. The value of ω_{Th} also affects the threshold depth of focus (z_r). Therefore, for clarity we present in Figure 4 a schematic diagram

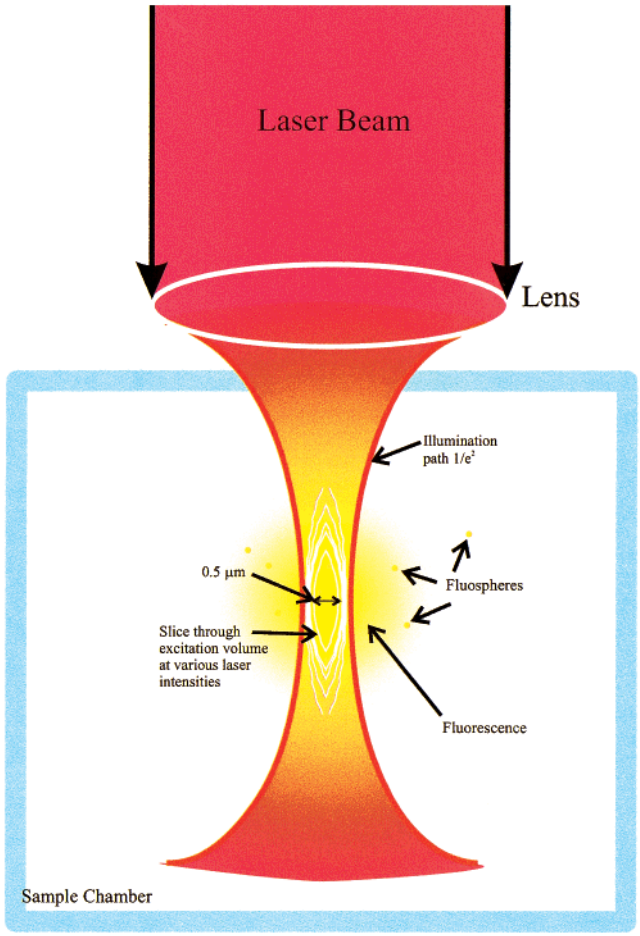

Figure 4. Schematic diagram of vertical slices through the excitation volume for increasing laser intensities. Also included are the $1/e^2$ border of the focused laser beam and a scale representation of the 100 nm nanospheres.

of vertical slices through the excitation volume over increasing laser intensities.

Although the predicted and measured beam waist agree to within experimental error, there appears to be a systematic deviation of the measured beam waist being smaller than the predicted values. This could arise from slight laser-induced local

heating, which causes the diffusion coefficient to increase with laser power. This would result in shorter transit times than predicted and therefore smaller apparent ω_{Th}'s. However, since this is speculative, we will not allow D to float in our data analysis (see next section).

Diffusion Coefficient. The diffusion coefficient for the 100 nm spheres was held fixed at 4.9×10^{-8} m^2/s for the power series experiments. In so doing, we assume only a negligible increase in solution temperature with increasing laser power. This is reasonable, because water absorbs very inefficiently at this wavelength ($\epsilon_{780} \cong 0.01$). Indeed, using thermal lens theory,[28] an increase of the local temperature in the laser volume is predicted to be less than 1 °C. This is in agreement with Denk et al.,[29] who considered the effect of local one-photon heating on multiphoton imaging in aqueous solution. Moreover, the intensities used in this experiment ($\leq 1 \times 10^{12}$ W/cm^2) are much less than those predicted by Xu and Webb (3×10^{13} W/cm^2)[30] to lead to the ionization of water and thus to heating of the solution through dielectric breakdown of the solvent.

As an aside, it is possible to fit our lower intensity data (32−66 mW) by allowing the diffusion coefficient to float. At the higher intensities (>90 mW), a flow term must be added to the ACF to fit the long lag time tail. However, when this is done and the effective temperature is calculated from the diffusion coefficient (assuming Stokes−Einstein diffusion applies), the temperature ranges from 40 to 70 °C. This seems highly unlikely in the absence of other evidence of high solution temperature, such as dissolved gas bubble formation. We therefore feel confident in holding D constant when analyzing our data.

Photodynamic Rate Constant. For the ACFs collected with laser intensity greater than 32 mW, a simple diffusion model could not fit the data. Instead, we include an exponential decay term in the model. Thus, eq 8 was used for modeling the data and was derived as previously described. Again in this model, we assume a nonrecoverable light-induced extinction of fluorescence. This is in contrast with intersystem crossing (blinking), which leads to a much different form of the ACF.[31,19] The average values of the count rate appears to be flat over the data collection time, because of the enormous "sink" of spheres found in the sample chamber, which is many orders of magnitude larger than the excitation volume. In the present work, the decay rate of the ACF increases with increasing laser intensity, although the excitation volume becomes larger. This implies that there is a dynamic process whose rate is a function of laser intensity. Examples of the modeled data can be found in Figure 5. In Figure 5a we include an attempted fit of eq 5 (i.e., simple diffusion) to the data. It is clear from this figure that eq 5 does not model the data adequately, because the ACF decay time is overestimated. In Figure 5b−f we include a photodynamic term resulting in a much better agreement between data and model. The recovered constants are collected in Table 1. Since the model represents the data very well, there is no reason to employ a more complex model for the ACF (i.e., including an intersystem crossing term). Indeed, it is unreasonable to expect single-molecule processes to be observable in our experiments as each sphere contains the order of 7400 dye molecules. Therefore, in order for intersystem crossing to be observable, thousands of dye molecules would have to undergo this process nearly simultaneously and at a rate much slower than previously observed for rhodamine dyes.[31] Permanent photobleaching of the dye is possible, but rhodamine dyes are very robust to photobleaching, and again, one would have to bleach a significant fraction the 7400 dye molecules within the sphere to observe this effect using FCS. Indeed, unpublished two-photon FCS data of single rhodamine molecules at high power have revealed no significant photobleaching.[32]

Examining the dependence of the rate constant on laser intensity may provide insight into the photodynamic process that we are measuring. If one assumes that there is a large excess of photons compared with absorbers then the process:

$$\text{sphere} + n \text{ photons} \Rightarrow \text{product (nonfluorescent)} \quad (11)$$

follows the rate equation:

$$\text{rate} = k'[\text{sphere}] \quad (12)$$

Where $k' = k$ [photons]^n. Thus, a plot of the natural logarithms of k' versus the laser intensity will have a slope of n (i.e., the number of photons involved in the process) and an intercept equal to the true value of the photodynamic rate constant. This plot is displayed in Figure 6. The slope was determined as 3.9 ($\pm$0.3) and k was found to be 1.1×10^{-7} M^{-4} s^{-1}. Therefore, we observe a photodynamic process, which is driven by the simultaneous absorption of four photons of wavelength 780 nm. The absorption would be either by polystyrene or the rhodamine-based fluorescence dye. This would lead to sphere destruction, dye photobleaching or both.

As previously noted, nonlinear laser ablation of polystyrene spheres has been observed by Misawa et al.[24] Using trapped 6 μm diameter spheres, they observed ablation effects from a single 355 nm laser shot of ~15 J cm^{-2} and complete sphere destruction for multiple laser shots on the trapped particle. Although our laser system delivers only ~10 nJ of energy per pulse, our strongly focused beam ($\omega_0 \approx 1$ μm) concentrates this energy into ~1 J cm^{-2}. Moreover, with multiple laser shots per transit time (8.2×10^4/ms), considerable energy could be deposited into a single sphere.

The possible photochemistry involved in sphere destruction also merits some discussion. A four 780 nm photon process delivers the equivalent of one 195 nm photon to the sphere. This wavelength has been shown to allow access into the S_3 state of polystyrene.[33] The possible photochemical outcomes of excitation into this state result from radical production, which may lead to cross-linking, double-bond formation or chain scission.[34] In both refs 32 and 33 double-bond formation was cited as one of the photoproducts, because the unloaded spheres became increasingly fluorescent upon exposure to radiation of $\lambda < 360$ nm. However, we observed no fourth-order laser power-dependent increase in fluorescence at any emission wavelength.

Since our spheres contain light-absorbing dye materials, we need to consider what effect this might have on the photodynamics, if any. From Figure 2, it is clear that the rhodamine dye molecules in our spheres initially undergo two-photon excitation that leads to fluorescence. This effect then begins to saturate at higher laser power (>90 mW), suggesting ground-state depletion.[19] It is possible that a "dark" four-photon process takes place where the dye is excited and then transfers energy to polystyrene. This would probably be a weak interaction, owing to the poor overlap of the emission spectrum of the dye and absorption spectrum of polystyrene, which is nonzero only at $\lambda < 340$ nm. It is also possible that the Stokes' shift between four-photon absorption and fluorescence emission results in the deposition of energy into the polystyrene matrix. This type of effect has been observed for single-photon excitation of

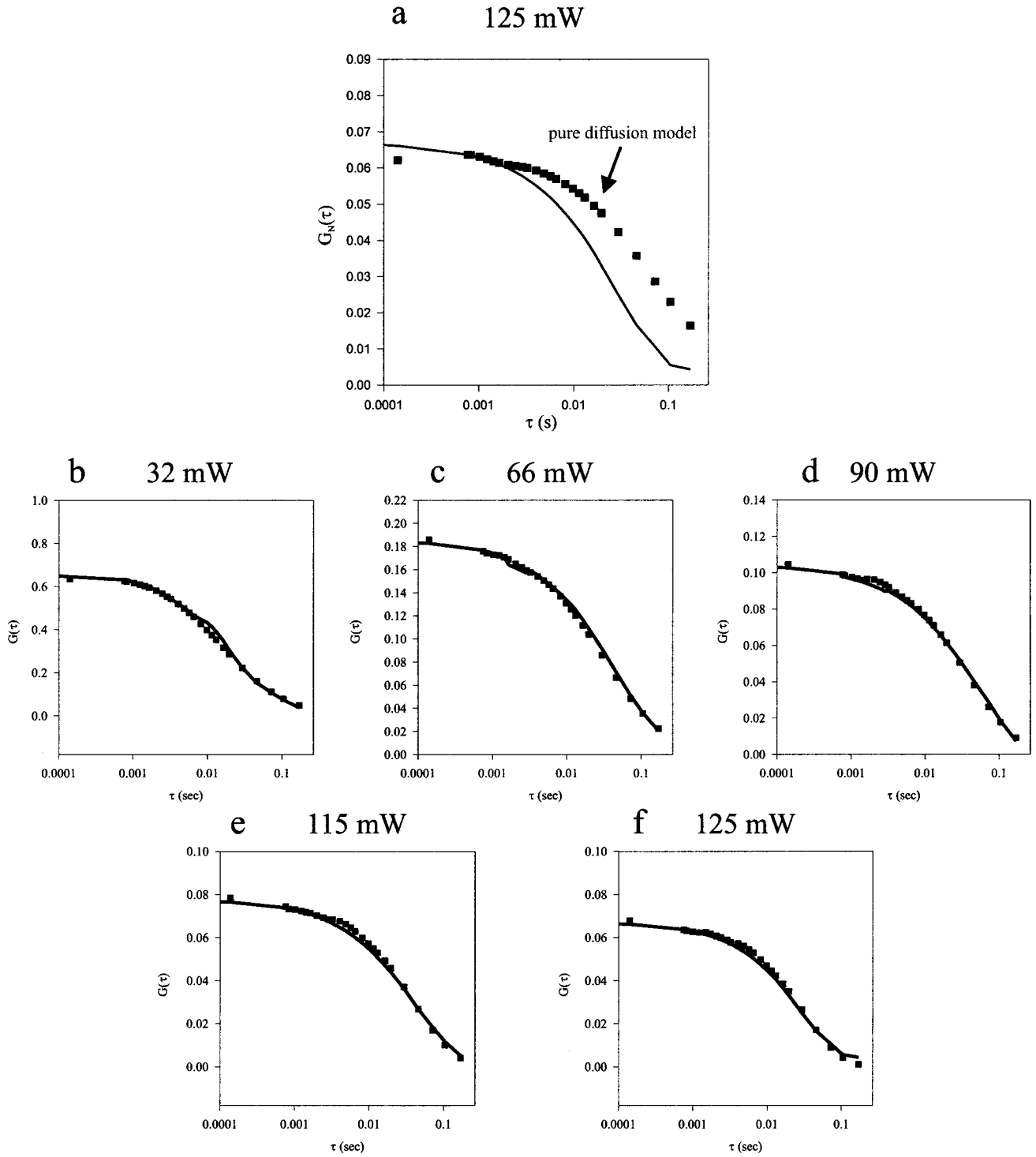

Figure 5. (a) The fluorescence autocorrelation function for laser intensity 125 mW (line) and the modeled data (squares) using eq 5 (i.e., simple diffusion). Note that the data and model disagree substantially for the decay time of the ACF. (b−f) Examples of the fluorescence autocorrelation functions (lines) and the modeled data (squares) for laser intensities of 32, 66, 90, 115, and 125 mW laser power. Here the model included a dynamic term (i.e., eq 8 or 10), resulting in a much better fit.

fluorescein- and nile red-containing polystyrene spheres.[33] However, if this were a dominant process in the present study, we would expect also to observe a dependence of the fluorescence signal on the fourth power of the laser intensity.

As discussed in the theory section, there are two possible origins of the exponential decay behavior of the ACF. These are light-induced photodestruction and flow. Since the nonrandom movement of spheres does not appear to arise from water heating-induced convection, the only other possibility is radiation pressure.[27] Radiation pressure is often cited as the force-generating phenomenon that is balanced with light gradient forces when a particle is optically trapped. When light reflects off an object, a momentum change imparts radiation pressure. Moreover, when an object absorbs a fraction of the incident light, radiation pressure dominates and an object is most likely to be accelerated by an intense, focused beam of light, such as a laser beam. Using eq 10, the resultant flow velocities span the range 4.0×10^{-6} m/s to 1.6×10^{-5} m/s. Similar to the analysis of the photodamage kinetics, a ln−ln plot of velocity versus laser power was constructed to evaluate the photon

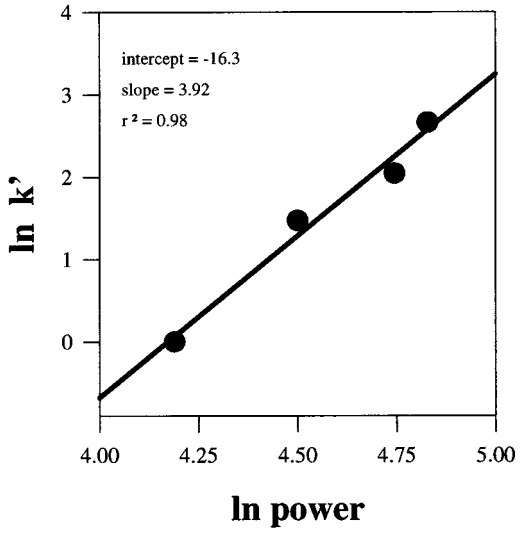

Figure 6. Plot of the natural logarithms of k' versus the laser intensities.

dependence of the flow velocity. Assuming that the velocity is a function of laser power, the slope of the plot suggests that the velocity varies as the laser power squared.

Although radiation pressure velocities of the order suggested here have been measured before,[35] we submit that this scenario is possible, but not dominant, in the present study for the following reasons. Drift is observed where a single particle is in the beam focus, which is not the case here. In fact, as the laser intensity increases, the number of particles in the excitation volume (i.e., at or near the beam focus) increases as can be observed from the $G_D^N(0)$ values. Radiation pressure induced by reflection from the sphere-buffer interface should result in a linear increase of velocity as a function of laser intensity[36] and we observe be a quadratic dependence. Furthermore, even if the radiation pressure depended quadratically on laser power (because of a convolution of the two-photon dye absorption into the radiation pressure model), the velocity should reach a maximum value, because the two-photon absorption saturates.

We must also consider the ramifications of optical trapping on the ACF. Although we use spheres that are smaller than those usually employed in trapping experiments, there remains a finite possibility that we trap some of the spheres. If significant trapping were occurring, then one would expect to observe the transit time lengthening with laser power, because a trapped particle has a longer residence time in the excitation volume. This is opposite to the present observations. If spheres are trapped in our experiments, the photodamage occurs too fast for the trapping event to be maintained for a significant period of time.

Conclusions

We have measured the photodynamic behavior of 100 nm polystyrene nanospheres in buffer solution using two-photon fluorescence correlation spectroscopy. The photodynamics manifest as a laser intensity dependent increase in the decay rate of the fluorescence autocorrelation. This behavior can be modeled assuming that the laser light induces a four-photon ablative process of the spheres. We found that while the solvent was not significantly affected by the high laser intensities used ($\sim 1 \times 10^{12}$ W/cm^2), refractive organic material was severely compromised. This suggests that similar processes will occur for multiphoton imaging at high laser fluences and in possibly pulsed femtosecond laser optical traps.

Acknowledgment. This work is supported by the Natural Sciences and Engineering Research Council of Canada and the Alberta Cancer Board. Financial assistance from the University of Calgary is also gratefully appreciated. RLG acknowledges the support of Nova Chemicals in the form of a graduate scholarship. We thank Professor Enrico Gratton for many helpful suggestions. We are indebted to Dave Malinsky and Teddi Mani of the University of Calgary for their help in the construction of the FCS apparatus. Professor G. Liu kindly donated time on his spectrofluorometer.

Appendix

Spectroscopic experiments usually involve the measurement of an appropriate correlation function; thus, in the case of fluorescence fluctuation spectroscopy it is the fluorescence autocorrelation function (ACF) $\langle \delta F(t)\delta F(t+\tau)\rangle$ that plays a central role. Here $\delta F(t) = F(t) - \langle F\rangle$ is the fluctuation in the measured fluorescence intensity $F(t)$ from its average value $\langle F\rangle$, $\langle\ \rangle$ represents an ensemble average, and t and $t+\tau$ are two points in time between which the correlation is studied. In some of the equations written below we will use the shorthand notation $t' \equiv t+\tau$. In this paper a two-photon excitation caused by a laser of intensity $I(\vec{r},t)$ and directed along the z axis of a Cartesian frame will be considered. The vector $\vec{r}(x,y,z)$ denotes a location within the experimental chamber with respect to the coordinate origin. The fluorescence intensity, $F(t)$, must, clearly, be related to both the intensity of the excitation and as well as the concentration of the molecules undergoing fluorescence. The detailed derivation of this relationship is well-known[1,5] and will not be discussed here; however, the final form of the fluorescence fluctuations can be written as:

$$\delta F(t) = \alpha \int \mathrm{d}\vec{r}\ I^2(\vec{r},t)\delta c(\vec{r},t) \qquad \text{(A.1)}$$

where, α is a constant and $\delta c(\vec{r},t)$ is a fluctuation in the concentration, $c(\vec{r},t)$, of the fluorescing molecules from its average value $\langle c\rangle$ given by $\delta c(\vec{r},t) = c(\vec{r},t) - \langle c\rangle$. The precise form of the function $I(\vec{r},t)$ is given in the main body of this paper in eq 1.

With these quantities the ACF is expressed in terms of the concentration auto-correlation function $f(\vec{r},\vec{r}',t,t+\tau)$ (CACF) as:

$$\langle \delta F(t)\delta F(t+\tau)\rangle = \alpha^2 \int d\vec{r}\, d\vec{r}\,' I^2(\vec{r},t) I^2(\vec{r}\,',t) f(\vec{r},\vec{r}\,',t,t+\tau) \qquad \text{(A.2)}$$

with:

$$f(\vec{r},\vec{r}\,',t,t+\tau) = \langle \delta c(\vec{r},t)\delta c(\vec{r}\,',t+\tau)\rangle \qquad \text{(A.3)}$$

where $\vec{r}(x,y,z)$ and $\vec{r}\,'(x',y',z')$ are two points within the experimental chamber. It is convenient to study the auto-correlation function in a Fourier transform space:

$$f(\vec{r},\vec{r}\,',t,t+\tau) = \int \frac{\mathrm{d}\vec{k}}{(2\pi)^3} \frac{\mathrm{d}\vec{k}'}{(2\pi)^3} \mathrm{e}^{i\vec{k},\vec{r}+i\vec{k}',\vec{r}\,'} f(\vec{k},\vec{k}',t,t+\tau) \qquad \text{(A.4)}$$

Here $f(\vec{k},\vec{k}',t,t+\tau) = \langle \delta c(\vec{k},t)\delta c(\vec{k}',t+\tau)\rangle$, where $\vec{k}$ and $\vec{k}'$ are the Fourier transform vectors. Physically, the CACF must obey the criterion of translational invariance and be independent of the origin of time (Stationarity). The former criterion requires the equality $\vec{k}' = -\vec{k}$ while the latter allows $t = 0$ resulting in a simplified form:

$$f(\vec{r},\vec{r}',0,\tau) = \int \frac{d\vec{k}}{(2\pi)^3} e^{i\vec{k}\cdot(\vec{r}-\vec{r}')} \langle \delta c(\vec{k},0)\delta c(-\vec{k},\tau)\rangle \quad (A.5)$$

To compute the auto-correlation function the Fourier transform, $\delta c(\vec{k},t)$, must be first calculated, which is achieved by assuming an equation of motion (generally, either the diffusion equation itself or its modification) for the concentration. If one suspects that the concentration of fluorescent species could be affected by a unidirectional chemical reaction- and radiation pressure-induced flow, then these phenomena can be represented in the equation of motion for concentration. These phenomena are represented by a velocity (v_z) term along the z-axis, and a kinetic term with rate constant, k_{PD}, (representing a photodynamic reaction)

$$\frac{\partial}{\partial t'}\delta c(\vec{r}',t') = D\nabla^2\delta c(\vec{r}',t') - v_z\frac{\partial}{\partial z'}\delta c(\vec{r}',t') - k_{PD}\delta c(\vec{r}',t') \quad (A.6)$$

To solve this equation we begin with a time dependent transformation:

$$\delta c(\vec{r}',t') = \delta\bar{c}(\vec{r}',t')e^{-k_{PD}t'} \quad (A.7)$$

This allows the reaction term to be eliminated leading to a simpler differential equation:

$$\frac{\partial}{\partial t'}\delta\bar{c}(\vec{r}',t') = D\nabla^2\delta\bar{c}(\vec{r}',t') - v_z\frac{\partial}{\partial z'}\delta\bar{c}(\vec{r}',t') \quad (A.8)$$

For $t = 0$ the correlation function defined in eq A.5 may now be written as

$$f(\vec{r},\vec{r}',0,\tau) = e^{-k_{PD}\tau}\int \frac{d\vec{k}}{(2\pi)^3} e^{i\vec{k}\cdot(\vec{r}-\vec{r}')}\langle\delta\bar{c}(\vec{k},0)\delta\bar{c}(-\vec{k},\tau)\rangle \equiv e^{-k_{PD}\tau}\bar{f}(\vec{r},\vec{r}',0,\tau) \quad (A.9)$$

The solution to eq A.8 in Fourier transform space can be obtained by using the standard methods and is of the form:

$$\delta\bar{c}(\vec{k},\tau') = \delta\bar{c}(\vec{k},t)\, e^{-[Dk^2+iv k_z](t+\tau)} \quad (A.10)$$

Here, k_z is the z-component of the vector $\vec{k}$. Substitution of eq A.10 in A.9 yields:

$$f(\vec{r},\vec{r}',0,\tau) = \langle c\rangle e^{-k_{PD}\tau}\int \frac{d\vec{k}}{(2\pi)^3} e^{i\vec{k}\cdot(\vec{r}-\vec{r}')}\, e^{-(Dk^2+iv k_z)\tau} \quad (A.11)$$

where $\langle c\rangle = \langle \delta c(\vec{k},0)\delta c(-\vec{k},0)\rangle$ and the form of this constant may be determined in the manner suggested by Thompson.[1]

Substitution of eq A.11 in eq A.2 along with the relevant definitions of the functions $I(\vec{r},t)$ and $I(\vec{r}',t)$ allows the integrations over the set of variables $\{x,x',y,y'\}$ to be explicitly carried out. The only remaining integrals are those over z and z' and a change in variables to a new set, S and u,

$$z = z_r\left(S - \frac{u}{\sqrt{2}}\right) + \frac{1}{2}v\tau \quad \text{and} \quad z' = z_r\left(S + \frac{u}{\sqrt{2}}\right) + \frac{1}{2}v\tau \quad (A.12)$$

allows eq A.2 to be written as

$$\langle \delta F(0)\delta F(\tau)\rangle = \beta\langle c\rangle e^{-(k_{PD}+v^2/4D)\tau}\int_{-\infty}^{\infty} du\, e^{-u^2/2D\tau + vu/2D}\int_{-\infty}^{\infty} dS\, \frac{1}{\Phi(u,S)} \quad (A.13)$$

where $\Phi(u,S)$ is a quadratic polynomial in the variable S and the relevant integration can be carried out by using Cauchy's theorem. The parameter β is a collection of well defined constants. Finally the integral takes the following form

$$\langle \delta F(0)\delta F(\tau)\rangle = \Omega e^{-(k_{PD}+v^2/4D)\tau}\int_{-\infty}^{\infty} du \frac{e^{-u^2/2D\tau + vu/2D}}{u^4 + (2 + 16D\tau/\omega_0^2)u^2 z_r^2 + \frac{1}{4}\left(\frac{16D\tau}{\omega_0^2}\right)^2 z_r^2} \left[\frac{2u^2 + \left(\frac{16D\tau}{\omega_0^2} - 4\right)z_r^2}{\sqrt{2}(4z_r^2 + u^2)} + \frac{2}{\left(u^2 + 2\left(2 + \frac{16D\tau}{\omega_0^2}\right)z_r^2\right)^{1/2}}\right] \quad (A.14)$$

where,

$$\Omega = \frac{2\alpha^2 I_0^4\,\omega_0^6}{\lambda^2\sqrt{4\pi D\tau}}\langle c\rangle \quad (A.15)$$

Equation A.14 is written in a form closely allied to that derived by Berland et al.[5] and reduces to it in the limit $k_{PD} \rightarrow 0$ and $v \rightarrow 0$. Moreover, If one chooses $v \rightarrow 0$ then the normalization of eq A.14 leads to eq 8 in the main body of the text, whereas if one chooses $k_{PD} \rightarrow 0$, then then the normalization eq A.14 leads to eq 10.

References and Notes

(1) Elson, E. L.; Magde, D. *Biopolymers* **1974**, *13*, 1.
(2) Thompson, N. L. *Topics in Fluorescence Spectroscopy 1*; Lakowicz, J. R., Ed.; Plenum: New York, 1991; Chapter 6.
(3) Rigler, R.; Widengren, J. *Bioscience* **1990**, *3*, 180.
(4) Widengren, J.; Rigler, R.; Mets, U. *J. Fluorescence* **1994**, *4*, 255.
(5) Berland, K. M.; So, P. T. C.; Gratton, E. *Biophys. J.* **1995**, *68*, 694.
(6) Brock, R.; Jovin, T. M. *Cell. Mol. Biol.* **1998**, *44*, 847.
(7) Widengren, J.; Rigler, R. *Cell. Mol. Biol.* **1998**, *44*, 857.
(8) Kinjo, M.; Rigler, R. *Nucleic Acids Res.* **1995**, *23*, 1795.
(9) Oehlenschlager, F.; Schwille, P.; Eigen, M. *Proc. Natl. Acad. Sci. U.S.A.* **1996**, *93*, 12811.
(10) Widengren, J.; Rigler, R. *J. Fluorescence* **1997**, *7*, 211S.
(11) Aich, P.; Nielsen, P.; Rigler R *Nucleosides Nucleotides* **1997**, *16*, 609.
(12) Sevenich, F. W.; Langowski, J.; Weiss, V.; Rippe, K. *Nucleic Acids Res.* **1998**, *26*, 1373.
(13) Politz, J. C.; Browne, E. S.; Wolf, D. E.; Pederson, T. *Proc. Natl. Acad. Sci. U.S.A.* **1998**, *95*, 6043.
(14) Starchev, K.; Buffle, J.; Perez, E. *J. Colloid Interface Sci.* **1999**, *213*, 479.
(15) Hasler, K.; Panke, O.; Junge, W. *Biochemistry* **1999**, *38*, 13759.
(16) Widengren, J.; Mets, U.; Rigler, R *Chem. Phys.* **1999**, *250*, 171.
(17) Tessier, A.; Meallet-Renault, R.; Denjean, P.; Miller, D.; Pansu, R. B. *Phys. Chem. Chem. Phys.* **1999**, *1*, 5767.
(18) Denk, W.; Strickler, J. H.; Webb, W. W. *Science* **1990**, *248*, 73.
(19) Schwille, P.; Haupts, U.; Maiti, S.; Webb, W. W. *Biophys. J.* **1999**, *77*, 2251.
(20) Eggeling, C.; Widengren J.; Rigler, R.; Seidel, C. A. M. *Anal. Chem.* **1998**, *70*, 2651.
(21) Konig, K.; So, P. T. C.; Mantulin, W. W.; Gratton, E. *Opt. Lett.* **1997**, *22*, 135.
(22) Konig, K.; Liang, H.; Berns, M. W.; Tromberg, B. J. *Nature* **1995**, *377*, 20.
(23) Zhang, Z.; Sonek, G. J.; Liang, H.; Berns, M. W.; Tromberg, B. J. *Appl. Opt.* **1998**, *37*, 2766.
(24) Misawa, H.; Koshioka, M.; Sasaki, K.; Kitamura, N.; Mashuhara, H. *J. Appl. Phys.* **1991**, *70*, 3829.
(25) Kogelnik, H.; Li, T. *Appl. Opt.* **1981**, *20*, 1550.
(26) Palmer, A. G.; Thompson, N. L. *Biophys. J.* **1987**, *51*, 339.
(27) Saski, K.; Tsukima, M.; Mashuhara, H. *Appl. Phys. Lett.* **1997**, *71*, 37.

(28) Kliger, D. S. *Ultrasensitive Laser Spectroscopy*; Academic Press: New York, 1983.

(29) Denk, W.; Piston, D. W.; Webb. W. W. In *Handbook of Biological Confocal Microscopy*; Pawley, J., Ed.; Plenum: New York, 1995; Chapter 28.

(30) Xu, C.; Webb. W. W. In *Topics in Fluorescence Spectroscopy 5*; Lakowicz, J. R., Ed.; Plenum: New York, 1997; Chapter 11.

(31) Widengren, J.; Rigler, R. *Bioimaging* **1996**, *4*, 149.

(32) Chen, Y.; Gratton, E., private communication.

(33) Simons, J. K.; Chem, J. M.; Taylor, J. W.; Rosenberg, R. A. *Macromolecules* **1993**, *26*, 3262−3266.

(34) Crawford, K. D.; Hughes, K. D. *J. Phys. Chem. B* **1997**, *101*, 864.

(35) Nemoto, S.; Togo, H. *Appl. Opt.* **1998**, *37*, 6386.

(36) Shen, Y. R. *The Principles of Nonlinear Optics*; Wiley: New York, 1984; Chapter 20.